

Large-Scale Outflows in Edge-on Seyfert Galaxies.

III. Kiloparsec-Scale Soft X-ray Emission

Edward J. M. Colbert^{1,2,3,4}, Stefi A. Baum¹, Christopher P. O’Dea¹, Sylvain Veilleux²

ABSTRACT

We present ROSAT PSPC and HRI images of eight galaxies selected from a distance-limited sample of 22 edge-on Seyfert galaxies. Kiloparsec-scale soft X-ray nebulae extend along the galaxy minor axes in three galaxies (NGC 2992, NGC 4388 and NGC 5506). The extended X-ray emission has 0.2–2.4 keV X-ray luminosities of $0.4\text{--}3.5 \times 10^{40}$ erg s⁻¹. The X-ray nebulae are roughly co-spatial with the large-scale radio emission, suggesting that both are produced by large-scale galactic outflows. Assuming pressure balance between the radio and X-ray plasmas, the X-ray filling factor is $\gtrsim 10^4$ times larger than the radio plasma filling factor, suggesting that large-scale outflows in Seyfert galaxies are predominantly winds of thermal X-ray emitting gas. We favor an interpretation in which large-scale outflows originate as AGN-driven jets that entrain and heat gas on kpc scales as they make their way out of the galaxy. AGN- and starburst-driven winds are also possible explanations in cases where the winds are oriented along the rotation axis of the galaxy disk.

Subject headings: kinematics and dynamics: galaxies — galaxies: Seyfert — galaxies: starburst — X-rays: galaxies

1. Introduction

Observations of sub-kpc radio structures in Seyfert galaxies have shown the presence of linear radio sources resembling jets from the active galactic nucleus (AGN; e.g., Ulvestad

¹ Space Telescope Science Institute, 3700 San Martin Drive, Baltimore, MD 21218

² Department of Astronomy, University of Maryland, College Park, MD 20742

³ NAS/NRC Research Associate

⁴ present address: Mail Code 662, Laboratory for High Energy Astrophysics, NASA Goddard Space Flight Center, Greenbelt, MD 20771

& Wilson 1989). Thus, it is known that *nuclear* outflows from the AGN are present in some Seyfert galaxies. It is possible that, in some galaxies, these nuclear outflows extend out of the galaxy disk and manifest themselves as *galactic* outflows, perhaps as lower-power versions of the ~ 10 – 100 kpc scale jets in radio galaxies and quasars. However, AGNs in Seyfert galaxies are weak optical and radio emitters (e.g., Antonucci 1993). In quasars, for example, emission from the AGN dominates over that produced by the host galaxy, but this may not be the case in some Seyfert galaxies. The host galaxies of Seyfert nuclei are capable of driving powerful starburst-driven galactic outflows, similar to those found in classical starburst galaxies (e.g., Heckman, Armus & Miley 1990) if the nuclear star formation rate is high enough (e.g., Heckman et al. 1995, Heckman et al. 1997). Therefore, kiloparsec scale radio structures in Seyfert galaxies (Baum et al. 1993; Colbert et al. 1996) could be produced by galactic outflows from a nuclear starburst or by nuclear outflows from the AGN.

We are currently conducting a research program to study the properties of these large-scale ($R \gtrsim 1$ kpc) outflows (LSOs) in Seyfert galaxies in order to investigate their nature and origin. We have selected a distance-limited sample of 22 edge-on Seyfert galaxies (see Colbert et al. 1996b, hereafter paper I) and have searched for emission from LSOs from these galaxies at optical (paper I) and radio wavelengths (Colbert et al. 1996a, hereafter paper II). In paper I, we showed that optical emission suggestive of LSOs was present in $\gtrsim \frac{1}{4}$ of all galaxies observed. In paper II, we found that kiloparsec-scale radio structures were present in $\gtrsim \frac{1}{2}$ of all galaxies observed. These results show that LSOs are quite common in Seyfert galaxies. In paper II, we also found that the radio structures have diffuse morphologies similar to bubbles or lobes and that the morphologies are generally different from a spherical halo structure that is observed in the starburst galaxy M82 (Seaquist & Odegard 1991). In the present paper, we present ROSAT soft X-ray (0.2 – 2.4 keV) images of eight of the 22 galaxies from the distance-limited sample in order to study the X-ray properties of LSOs in Seyfert galaxies.

The observational data and data reduction are described in section 2 and the images and results are presented in section 3. In section 4, we discuss the properties of the extended X-ray emitting gas. Implications on the nature of LSOs in Seyfert galaxies are discussed in section 5. A summary is given in section 6.

2. Observations and Data Reduction

For ease of reference, in Table 1, we list the 22 Seyfert galaxies from the edge-on sample (paper I) and their assumed distances. The NASA HEASARC database of all

pointed ROSAT observations was used to select public archival data, taken with either the Position-Sensitive Proportional Counter (PSPC) or High-Resolution Imager (HRI). Data were available for ten of the 22 galaxies listed in Table 1. The selected data were retrieved from the U. S. ROSAT archives at NASA’s Goddard Space Flight Center.

A list of the archival ROSAT data is given in Table 2. For each observation, we list the offset of the optical position of the galaxy (see paper I, Table 1) from the pointing center, date of the observation, instrument used, exposure time, net counts and net count rates from the galaxy. Net counts were calculated by extracting source counts from circular regions of radius $1'$ and background counts from source-free regions surrounding the X-ray source (typically circular annuli). NGC 4945 has a very large angular size compared to the other galaxies. For this galaxy, we used a rectangular source region of width $7.4'$ and length $21.6'$ oriented along PA 42° . For comparison, we also list (Table 2, column 8) the expected count rate for a hypothetical source with a $0.2\text{--}2.4$ keV luminosity of 10^{40} erg s^{-1} and a thermal spectrum with temperature $kT = 1.0$ keV with absorption from cold gas in our Galaxy. This luminosity and spectrum are typical of a starburst-driven galactic outflow (e.g., Armus et al. 1996) and of what might be expected from an LSO. Count rates were calculated with the XSPEC X-ray spectral fitting software package, using the Galactic absorption columns listed in column 9. Note that the hypothetical “ 10^{40} erg s^{-1} ” LSO count rates are comparable in magnitude to the uncertainties in the total count rates (column 7), so it is necessary to spatially resolve sources with luminosities $\sim 10^{40}$ erg s^{-1} in order to detect them.

The point-spread functions of the PSPC and HRI are dependent on the X-ray spectrum, but typical Gaussian core widths are $20\text{--}30''$ and $7\text{--}10''$ full-width half-maximum (FWHM), respectively. Although the PSPC has poorer resolution, it is much more sensitive than the HRI, due to its very low internal background count rate. The energy range of both instruments is $\sim 0.2\text{--}2.4$ keV. Approximate total background rates for the two instruments are 1.4 and 3.8×10^{-3} counts s^{-1} arcmin $^{-2}$, for the PSPC and HRI, respectively.

It is instructive to compare the background count rate in a detect cell to the hypothetical “ 10^{40} erg s^{-1} ” LSO count rates listed in Table 2, column 8. For the PSPC, $\sim 90\%$ of the source counts fall within radius $23''$, so that we expect a background count rate of 0.06×10^{-2} s^{-1} in a detect cell. This is much lower than the hypothetical “ 10^{40} erg s^{-1} ” count rates, so the PSPC data are easily sensitive to LSO X-ray emission, as long as the emission can be resolved from the nuclear source. For the HRI, $\sim 90\%$ of the source counts fall within a radius of $\sim 10''$, so the expected background count rate in a $\sim 10''$ radius detect cell is 0.03×10^{-2} s^{-1} . Again, in all cases, 10^{40} erg s^{-1} emission from an LSO would be detected as long as it is resolved from the nuclear source.

Two (NGC 4602 and NGC 7410) of the ten galaxies were not detected (count rate $\lesssim 2\sigma$ above the background using a $1'$ radius detect cell). By comparing the upper limits to the count rates (Table 2, column 7) with those of the hypothetical “ 10^{40} erg s^{-1} ” source (Table 2, column 8), we note that the total 0.2–2.4 keV luminosities of these two galaxies are less than several $\times 10^{40}$ erg s^{-1} .

Images of the remaining eight galaxies were made using the PROS X-ray reduction software in IRAF. First, the raw images were binned by a factor of 8 to make new images with $4''$ pixels. These images were then smoothed with a Gaussian kernel of $\sigma = 24''$. For the HRI data, higher resolution images were also made by smoothing with a Gaussian kernel of $\sigma = 8''$.

In Table 3, we list the eight galaxies for which contour maps are presented, along with the angular size of 1.0 kpc at the assumed distance and the figure number of the contour map of the image. Note that for most of the galaxies, the PSPC resolution of $\sim 25''$ is too poor to resolve any emission within ~ 5 kpc. The HRI resolution is significantly better. Contour levels for all plots are in units of counts pixel^{-1} (225 counts arcmin^{-2}).

We do not attempt to model the spectra of the X-ray data. The relatively low number of total counts and inadequate energy range ($\lesssim 2.4$ keV) of the PSPC detector make spectral fitting a two-component model (e.g., a power-law for the AGN and a thermal spectrum for the LSO) infeasible. Although the HRI is capable of resolving extended emission from the LSO, the pulse height amplitude (PHA) channels of the HRI are not calibrated very well in energy, so it is not possible to estimate the temperature of any resolved thermal emission from the HRI observations.

3. Results

Here we present and discuss the ROSAT HRI and PSPC soft X-ray images for individual Seyfert galaxies in the edge-on sample.

3.1. Individual Objects

NGC 2992. The HRI image of NGC 2992 was previously published by Weaver et al. (1996), but they did not note the presence of any extended X-ray emission. In Figure 1a, we show a contour map of the HRI image of NGC 2992. It is immediately obvious that the companion galaxy NGC 2993 is also a source of soft X-ray emission. It is also clear that soft X-ray emission extends out to $\sim 1'$ (~ 9 kpc) to the southeast in PA $\sim 100^\circ$, roughly along

the galaxy minor axis. Although the PSPC image (not shown) is much more sensitive to faint emission, the strong emission from the nuclear source dominates the image and thus no extended emission is resolved.

NGC 4235. The X-ray source in both (1992 June and 1992 December) PSPC images of NGC 4235 is unresolved. The PSPC resolution of $\sim 25''$ corresponds to ~ 3.9 kpc and the X-ray emission from the nuclear source certainly dominates over any possible extended X-ray emission on kpc scales.

NGC 4388. The HRI image of NGC 4388 was previously published by Matt et al. (1994). These authors found extended emission out to radii $\sim 45''$ (7.3 kpc), roughly evenly distributed over all azimuthal angles. Contour maps of the HRI and PSPC images are shown in Figures 1b and 1c, respectively. In the PSPC image, we note the presence of a larger scale X-ray structure, extending out to radii $\sim 2'$ (19.5 kpc) in P.A. $\sim 65^\circ$.

NGC 4602. A field near NGC 4602 was observed with the PSPC, but NGC 4602 was not detected. Unfortunately, during the observation, NGC 4602 was offset $\sim 19.2'$ from the center of the field of view, which is near the support ring on the PSPC detector.

NGC 4945. In Figure 1d, we show a contour plot of the 1992 August PSPC image of NGC 4945, overlaid on a grayscale plot of the optical emission. NGC 4945 is very near the Galactic plane ($b \approx 13^\circ$) and, consequently, the Galactic absorbing column is quite large ($N_H \sim 1.5 \times 10^{21} \text{ cm}^{-2}$, Table 2). Thus, soft X-ray emission below $\sim 1\text{--}2$ keV will be severely absorbed in the image. No extended soft X-ray emission is evident in the 1993 July PSPC image either.

IC 4329A. This galaxy is located at a distance of ~ 64 Mpc, at which the PSPC resolution of $\sim 25''$ corresponds to ~ 7.8 kpc. More complications arise because this type 1 Seyfert nucleus is a very luminous X-ray source and photons within radii $\sim 2'$ (corresponding to physical distances $\lesssim 35$ kpc) are dominated by the unresolved nuclear source. A contour plot of the PSPC image is shown in Figure 2a.

NGC 5506. In Figure 2b, we show a contour map of a PSPC image of NGC 5506. Note that it appears to be extended along P.A. $\sim 150^\circ$, roughly the same orientation as the large-scale radio emission (paper II). On smaller scales, as shown in the HRI image (Figure 2c), the emission is extended in roughly the same P.A.

ESO 103-G35. The galaxy ESO 103-G35 was observed with the PSPC, but very few (~ 73) net counts were detected. We do not find any evidence for extended X-ray emission.

NGC 7410. The PSPC observation of the galaxy NGC 7410 was quite short (~ 1 ksec) and there were only 7.4 ± 5.5 net counts from the galaxy, too weak to claim a definite

detection.

NGC 7590. The PSPC observation of NGC 7590 was also quite short and we do not find any evidence for extended emission in the image.

3.2. Suitability of Imaging Data for Detecting Emission from LSOs

As mentioned in section 2, all of the images are sensitive to soft X-ray luminosities of $\sim 10^{40}$ erg s $^{-1}$, comparable to what would be expected from an LSO. Thus, the only issue with respect to the suitability of the data for detecting extended emission from LSOs with luminosities $\gtrsim 10^{40}$ erg s $^{-1}$ would be whether the emission can be resolved from the bright nuclear X-ray source. As can be seen from the angular scales listed in Table 3, the PSPC image of only one galaxy (NGC 4945) has spatial resolution suitable for resolving sources on scales ~ 1 – 2 kpc. The three HRI images of NGC 2992, NGC 4388 and NGC 5506 also have suitable resolution for imaging emission on scales $\gtrsim 1$ kpc.

Although the spatial resolution of the PSPC images is ~ 3 – 5 times worse than the HRI, the PSPC images are useful for searching for very extended X-ray emission, such as that in NGC 4388. For example, the PSPC images of NGC 2992, NGC 4235, NGC 4388, NGC 4945, NGC 5506 and NGC 7590 are sensitive to emission on size scales $\gtrsim 3$ – 5 kpc.

In summary, ROSAT imaging data suitable for searching for emission from LSOs on scales $\gtrsim 1$ kpc were available for four of the eight galaxies, and data suitable for searching for emission $\gtrsim 3$ – 5 kpc were available for six of the eight galaxies. For comparison, large-scale radio structures from LSOs have typical radii of ~ 1 – 5 kpc (paper II).

3.3. Extended Emission in NGC 2992, NGC 4388 and NGC 5506

As mentioned in section 3.1, three (NGC 2992, NGC 4388 and NGC 5506) of the galaxies show extended emission at radii $\gtrsim 1$ kpc. Ideally, one would like to make an image of the extended emission by subtracting the unresolved nuclear source. Unfortunately, this is not a straightforward procedure as the point-spread functions for both instruments are dependent on the energy spectrum of the source (especially for the PSPC). In addition, especially important for the HRI, an uncertainty in the aspect solution returned by the spacecraft introduces non-axisymmetric errors on size scales of ~ 5 – $10''$. Subtraction of the nuclear source could be attempted if there is a bright unresolved X-ray source near the pointing center that can be used as a point-spread function, but such sources were not present in the ROSAT images of these galaxies. Aspect errors can be reduced using

sophisticated image reconstruction methods (e.g., Morse 1994); however, these methods were not found to be very effective for these observations, due to the relatively low number of total counts. In the following subsections, we describe measurements of the net counts of the extended soft X-ray emission in these three galaxies.

3.3.1. NGC 2992

The extended emission in NGC 2992 (Figure 1a) extends along PA 112° , but does not appear extended along other PAs. The surface brightness of the extended emission in the HRI image is only slightly brighter than that from the wings of the unresolved nuclear source. In order to make evident the faint extended emission, in Figure 3, we show radial profiles of the X-ray emission in four quadrants (PA = $-30 - 60^\circ$, $60 - 150^\circ$, $150 - 240^\circ$, and $240 - 330^\circ$). The radial profile for the second quadrant (as listed above) is significantly peaked above the others (which serve as model PSFs) between $\sim 35''$ and $45''$. This excess is noticeable in radial profile plots binned at either 10 or 20 photons per radial bin, i.e., it is not a chance surplus of photons caused by binning the data (see Figure 3). For example, between radii $35''$ and $45''$, there are 20 total counts in the second quadrant and 27 total counts from *all three other quadrants together*. After background subtraction, the net number of counts of this extended emission in the second quadrant is 11.0 ± 4.8 .

3.3.2. NGC 4388

As noted in Table 2, relatively few source counts were detected in the data. The HRI image (Figure 1b) appears extended, but only ~ 150 counts are present in the raw image. The PSPC image also shows extended emission, is more sensitive, and contains more counts in the raw image. We use this image to estimate the count rate of the extended emission. In order to verify that the extended emission was not due to ‘ghost images’ of very soft ($E \lesssim 0.2$ keV) photons (Nousek & Lesser 1993), we omitted photons from PI channels 16 (of 256) and below. The total number of counts within a circle of radius $1'$ (which encloses $>95\%$ of the total counts from a point source) is 441. The total counts within a tilted rectangular region of width $2.5'$ and length $4.1'$, oriented along PA 46.5° (enclosing the whole galaxy) is 784, a difference of 343 counts. After subtraction of the background photons, this becomes 113 net counts. Although the central source may be contributing some of the photons beyond radii $1'$, this amounts to less than 5% of 339 net (background subtracted) counts, or less than 17 photons. Taking this uncertainty into account, the net counts and

uncertainty of the extended X-ray emission is 113 ± 28 .¹

3.3.3. NGC 5506

As can be seen in Figure 2c, the extended emission surrounding the central X-ray source in NGC 5506 is oriented along PA $\sim 160^\circ$, but has a rather large opening angle. In Figure 4, we show a radial profile of the counts per unit area, binned so there are at least 20 photons for each data point. Since the extended emission in NGC 5506 is directed over a large range in PA, we cannot easily use radial profiles in other PA ranges to model the PSF (as we did for NGC 2992). Instead, for comparison, we also plot the radial profile from a deep observation (106,359 net counts) of the point source HZ43, taken from a ROSAT HRI calibration observation (ROSAT sequence number RH141873N00). The HZ43 profile has been normalized to the NGC 5506 profile by dividing by the ratio of the total number of counts $\text{area}^{-1} \text{time}^{-1}$ for NGC 5506 to that of HZ43. The area used was that within radius $10''$.

NGC 5506 begins to show an increased X-ray surface brightness above the HZ43 PSF beyond radius $\sim 5''$. As noted above, the aspect solutions for HRI observations can produce errors on $\sim 10''$ scales, so it is not clear whether the apparent extent between 5 and $10''$ is real. However, the excess emission becomes even more pronounced between radii $\sim 10''$ and $25''$, which is not due to improper aspect solution. A conservative estimate of the net extended counts, calculated by subtracting the total counts from NGC 5506 between 10 and $25''$ from that of the normalized HZ43 distribution, is 72 ± 13 .

3.3.4. X-ray Luminosities of the Extended Soft X-ray Emission

In Table 4, we list ranges of the size of the extended emission in the three galaxies. Also listed is the range in PA over which the emission is extended, the net counts, and the net count rates of the extended emission.

Estimating fluxes and luminosities of the extended emission requires knowledge about the intrinsic spectrum of the emission. We assume a thermal spectrum (Raymond & Smith 1977) with absorption due to cold gas in our Galaxy. In Table 5, column 4, we list 0.2–2.4

¹ Approximately the same number of net photons was found if all PI channels were used (114 ± 29), indicating that ‘ghost images’ from very soft photons are not a significant factor in producing the observed extended emission.

keV luminosities of the extended emission for assumed thermal spectra for two sample plasma temperatures: (1) $kT = 0.1$ and (2) $kT = 1.0$ keV. We have used the X-ray spectral fitting program XSPEC to calculate X-ray fluxes from PSPC and HRI count rates, using the Galactic absorption columns listed in Table 2.

4. Nature of Extended Soft X-ray Emission

4.1. Emission Mechanism

We explore several possibilities for the emission mechanism producing the observed soft X-rays.

4.1.1. Scattered Nuclear Emission

The extended soft X-ray emission originates from regions $\gtrsim 1$ kpc from the nucleus, so it is not likely to be scattered X-rays from the nuclear X-ray source. The electron-scattering region in Seyfert galaxies is estimated to be ~ 1 pc (e.g., Krolik & Begelman 1986).

4.1.2. Synchrotron Emission

In bright jets such as that in M87, soft ($E \sim 1$ keV) X-ray emission from knots or hotspots is consistent with synchrotron emission (e.g., Biretta 1993). The expected synchrotron luminosity in the ROSAT (0.2–2.4 keV) band from a synchrotron source with 6 cm radio luminosities comparable to the large-scale radio structures in Seyfert galaxies ($\sim 10^{21}$ W Hz $^{-1}$; paper II) is $\sim 10^{40}$ erg s $^{-1}$ (assuming the synchrotron luminosity $L_\nu \propto \nu^{-0.7}$), which is comparable to the observed ROSAT X-ray luminosities. However, the lifetime of the relativistic electrons which would produce such high energy X-ray synchrotron emission is much shorter than that of electrons producing cm-wave radio emission. Specifically, the lifetimes are a factor $[\nu(\text{X-ray})/\nu(\text{radio})]^{0.5}$ shorter. This means that the electrons emitting 1 keV synchrotron emission live $\sim 10^{-4}$ as long as the ones emitting at 6 cm, or $\sim 10^3$ yrs, based on the 6 cm radio synchrotron lifetimes of the large-scale radio structures (paper II). Since there is no evidence on kiloparsec scales for a source that would supply relativistic electrons (e.g., a jet), we disregard synchrotron emission as a possible emission mechanism.

4.1.3. X-ray Point Sources in the Galaxy Halos

Since the X-ray luminosities of the extended emission is $> 10^{40}$ erg s^{-1} (Table 5), over 100 X-ray binaries emitting at 10^{38} erg s^{-1} would be required to provide enough X-ray emission. Such a large number of very luminous X-ray binaries is not expected in a galaxy halo. Although some X-ray supernovae emit with X-ray luminosities $\sim 10^{40}$ erg s^{-1} (e.g., Ryder et al. 1993), such objects are quite rare. The fact that the extended X-ray emission is roughly co-spatial with large-scale diffuse radio emission (section 4.3) argues that hot plasma in an LSO is producing extended, *diffuse* X-ray emission.

4.1.4. Thermal Emission from a Hot Plasma

Gas at temperatures $\sim 10^6$ – 10^7 K emits soft X-rays in an energy range in which the ROSAT detectors are quite sensitive. Our present ROSAT data are not suitable for measuring the temperature of the extended X-ray emission, so we have not attempted to do so. A thermal plasma with a temperature kT as low as ~ 0.1 keV or as high as several keV could be producing the soft X-rays. Wind shocks could heat gas to these temperatures. The temperature of gas which has been heated by a shock with velocity v is

$$kT = \frac{3}{16} \mu m_H v^2,$$

where μ is the mean atomic weight of the gas and m_H is the mass of the hydrogen atom. For shocks with velocities ~ 100 – 200 km s^{-1} the shocked gas will emit at temperatures $\lesssim 0.05$ keV, which is too low to be detected with ROSAT. However, wind shocks with velocities $\gtrsim 300$ – 1000 km s^{-1} will heat gas to temperatures of ~ 0.1 – 1.0 keV, which is in the ROSAT bandpass. An example of extended soft X-ray emission from a thermal plasma occurs in the Seyfert galaxy NGC 2110, in which the plasma temperature is ≈ 1 keV (Weaver et al. 1995). Since the extended emission in NGC 2992, NGC 4388 and NGC 5506 is positioned out of the galaxy disk (and therefore is not likely to be emission from sources in the galaxy disk), we favor an interpretation as thermal emission from a hot plasma with temperature $\sim 10^6$ – 10^7 K ($kT \sim 0.1$ – 1.0 keV).

4.2. Derived Properties

In Table 5, for each of the three galaxies with extended emission, we list important properties of the extended X-ray gas for two sample plasma temperatures: $kT = 0.1$ and

1.0 keV. The soft X-ray luminosity L_X in the ROSAT band (0.2–2.4 keV) is given by

$$L_X = \int n^2 \Lambda_X dV,$$

where n and V are the density and volume of the emitting gas and Λ_X is the emissivity of a thermal plasma (Raymond & Smith 1977) for the ROSAT bandpass. The X-ray emissivity is nearly constant over the ROSAT energy bandpass and we have used a value of $\Lambda_X = 10^{-22.4}$ erg cm³ s⁻¹, as given in Suchkov et al. (1994). The volume (Table 5, column 2) of the emitting region was calculated assuming a conical region with inner and outer radii and opening angle as given in Table 4.

$$V = \frac{2\pi}{3}[1 - \cos \alpha](R_{outer}^3 - R_{inner}^3),$$

where α is the half-angle of the cone.

We assume the hot plasma fills the emitting volume with filling factor f and list values of $f n^2 V = L_X / \Lambda_X$ in Table 5, column 5. We then calculated densities ($f^{1/2} n = (L_X / \Lambda_X V)^{1/2}$; column 6), pressures ($f^{1/2} 2nkT$; column 7), and cooling times of the hot gas. The cooling times have been calculated from the following formula:

$$t_{cool} \approx \frac{nkTfV}{L_X} = kTf^{1/2} \left(\frac{V}{\Lambda_X L_X} \right)^{1/2}.$$

4.3. Associated Radio Emission

In all three galaxies with extended X-ray emission, there is strong evidence for a large-scale outflow from both radio and optical observations (papers I and II). It is also noteworthy that the extended X-ray nebulae are roughly cospatial with the extended radio emission (see Figures 5 and 6), which is further evidence that the X-ray emission is produced by the galactic outflow.

5. Nature of Large-scale Outflows in Seyfert Galaxies

5.1. Frequency of Occurrence

Of the four galaxies in our sample for which ROSAT images with suitable sensitivity and ~ 1 kpc spatial resolution were available (see section 3.2), kpc-scale soft X-ray nebulae were found in three (NGC 2992, NGC 4388 and NGC 5506) of the galaxies. Although the eight objects observed make up an unbiased subsample of the distance-limited sample,

the sample of four objects for which suitable deep observations were made are probably biased. All three of these galaxies were previously known to have extended optical and radio emission. Thus, the 75% detection rate for extended X-ray emission may be an overestimate. However, it is noteworthy that the deep ROSAT observations strongly reinforce the presence of LSOs in these galaxies, confirming the evidence provided by optical and radio observations.

Wilson (1994) shows that at least four of six Seyfert galaxies studied in their research program show spatially extended soft X-ray emission. This suggests that extended soft X-ray emission from LSOs is common in Seyfert galaxies. Since LSOs are so common, the soft X-ray emission from LSOs could, in some cases, explain the “soft excess” component observed in total aperture X-ray spectra of Seyfert galaxies, which is present in $\gtrsim 50\%$ of Seyfert galaxies (e.g., Turner et al. 1991).

A systematic study of the frequency of occurrence of X-ray halos in edge-on normal and starburst galaxies has not been done. ROSAT X-ray luminosities of halos that have been detected in normal and starburst galaxies are \sim several $\times 10^{39}$ erg s $^{-1}$ (see, e.g., Bregman & Houck 1997), which is a factor of ~ 10 or more smaller than the luminosities of the extended emission we find in our study of Seyferts. This may indicate that there are two different types of outflows occurring. It would be interesting to compare the results of a study of normal and starbursting galaxies with our results for Seyfert galaxies.

5.2. Physical State of the Outflowing Gas

We can investigate the state of the gas in the LSOs by comparing the implied pressures and filling factors of the optically-emitting gas, the radio plasma, and the X-ray plasma. First we compare the optical and X-ray emitting gas. Optical line ratios from emission-line clouds at distances $\lesssim 1$ kpc from the Seyfert nucleus (in the so-called extended narrow-line region [ENLR]) suggest that the clouds have electron densities $n_e \sim 10^2 - 10^3$ cm $^{-3}$ and temperatures $T_e \approx 10^4$ K (e.g., Robinson 1989, Robinson 1994), implying pressures $n_e kT \sim 10^{-10} - 10^{-9}$ dyne cm $^{-2}$. We found that the extended X-ray emission from NGC 2992, NGC 4388 and NGC 5506 is located at larger radii (between ~ 2 and 13 kpc.) Since the pressure of outflowing wind gas is expected to drop as R^{-2} , the pressures of hot X-ray gas at the smaller radii of the ENLR clouds (~ 1 kpc) will be higher than those listed in Table 5. For example, LSO gas with pressures $\sim 10^{-12} - 10^{-10.1} f^{-\frac{1}{2}}$ dyne cm $^{-2}$ (the range for the three galaxies listed above; Table 5) at a sample radius of 5 kpc will have higher pressures $\sim 10^{-10.6} - 10^{-8.7} f^{-\frac{1}{2}}$ dyne cm $^{-2}$ at ~ 1 kpc. These pressures are roughly consistent with the electron pressures of the ENLR gas at the same radii ($\sim 10^{-10} - 10^{-9}$ dyne cm $^{-2}$). Thus,

if the X-ray gas and the ENLR clouds are in pressure equilibrium, then the X-ray filling factor $f \sim 0.1-1$.

Next, we compare the radio-emitting plasma with the X-ray plasma. The minimum-energy magnetic pressures of the large-scale radio structures imply that the kpc-scale *radio plasma* has pressures $\sim 10^{-14}-10^{-13} \phi^{-\frac{4}{7}}$ dyne cm^{-2} , where ϕ is the volume filling factor of the radio plasma (paper II). Assuming pressure balance between the X-ray and radio-emitting plasmas (a reasonable assumption since the large-scale X-ray and radio structures are roughly co-spatial), the ratio of filling factors $\phi/f \lesssim 10^{-4}$, i.e., there is heavy mixing of thermal gas within the radio-emitting volume or the radio plasma is confined to filamentary (or shell-like) regions.

In summary, our results suggest that the outflowing material in the LSOs of Seyfert galaxies is primarily composed of hot, thermal X-ray emitting gas (with only a small contribution of synchrotron-emitting relativistic electrons). The radio and X-ray plasmas are assumed to be in rough pressure equilibrium with the optical ENLR clouds. Krolik & Vrtilik (1984) describe a scenario in which the ENLR clouds in fact condense out of outflowing wind gas and create a two-phase medium in the ENLR, which is consistent with our results.

5.3. Possible Scenarios for LSOs in Seyfert Galaxies

In paper II, we noted that the large-scale radio structures in galaxies in our sample had diffuse morphologies, but that the morphologies did not resemble radio halos in starburst galaxies (like M82). We concluded that LSOs are most easily understood as AGN-driven outflows that are somehow diverted away from the galaxy disk on scales $\gtrsim 1$ kpc. Various mechanisms (e.g., cloud collisions, bending by ram pressure forces, and buoyancy forces) may act to divert the outflows as they blow outward from the nuclear region.

In the present paper, we find that LSOs are primarily composed of hot, X-ray emitting plasma, which suggests that, on kpc-scales, the outflows are more similar to wide-angled winds than to radio plasma jets from the AGN. A possible explanation is that AGN-driven jets entrain large amounts of gas as they make their way out of the galaxy. The entrained gas could be shock-heated to temperatures $\gtrsim 10^6$ K by winds with velocities $\gtrsim 300$ km s^{-1} .

Another possibility is that the outflows originate as winds very close to the nucleus. If the jets are stopped at small radii from the nucleus, the kinetic energy of the jet may become thermalized and heat the gas in the nuclear region (as does a compact starburst for a starburst-driven wind, see Heckman, Armus & Miley 1990). The high-pressure region can

then blow out of the galaxy disk in a wind. A nuclear starburst can also power a galactic wind in a Seyfert galaxy, if the nuclear star-formation rate is high enough. In the wind scenario, the large-scale X-ray and radio structures would tend to be oriented perpendicular to the galaxy major axis, which is the case for some LSO Seyfert galaxies (e.g., NGC 4388).

Detailed studies are needed to determine which energy source (AGN or nuclear starburst) dominates the energy input to the LSO in any given galaxy.

6. Summary

ROSAT PSPC and HRI soft X-ray imaging data for ten of the 22 galaxies from the complete sample were retrieved from the ROSAT archives and analyzed. Eight of these galaxies were detected. Suitable data for detecting extended soft (0.2–2.4 keV) X-ray emission on size scales $\gtrsim 1$ kpc were available for four galaxies and extended soft X-ray emission was found in three (NGC 2992, NGC 4388 and NGC 5506) of these four galaxies. The extended soft X-ray emission has 0.2–2.4 keV X-ray luminosities between 0.4 and 3.5×10^{40} erg $^{-1}$. Each one of these three galaxies also has strong evidence for a large-scale outflow from previous optical and/or radio observations (papers I and II). The large-scale radio, optical and X-ray emission is roughly co-spatial, and the soft X-ray emission is most plausibly explained by thermal emission from a gas in a galactic outflow. Assuming pressure balance between the radio and X-ray plasmas, the filling factor of the X-ray emitting gas is $\gtrsim 10^4$ times larger than that of the radio plasma. Large-scale outflows in Seyfert galaxies are most easily explained as wide-angled winds (as opposed to collimated jets) of hot, X-ray emitting gas that blow away from the nuclear region. We favor an interpretation in which LSOs originate as AGN-driven jets that entrain and heat gas on kpc scales as they make their way out of the galaxy. An alternate explanation is that LSOs originate as winds on small scales and this could be occurring in galaxies in which the LSOs are oriented roughly perpendicular to the galaxy major axis.

E.J.M.C. thanks Kim Weaver, Michael Dahlem and Martin Elvis for providing information and for helpful discussions and Michael Corcoran for helping with the NASA/HEASARC data archive. E.J.M.C. acknowledges support from the Director’s Office of the Space Telescope Science Institute, NASA grant NAG5-3016, and the National Research Council. S.V. acknowledges the financial support of NASA through grant LTSA 035-97. This research has made extensive use of the NASA/IPAC Extragalactic Database (NED), which is operated by the Jet Propulsion Laboratory, Caltech, under contract with NASA. The Digitized Sky Surveys were produced at STScI under U.S. Government grant

NAGW-2166. This paper represents a portion of E.J.M.C.'s Ph.D. thesis, submitted in partial fulfillment of the requirements of the Graduate School of the University of Maryland.

Table 1. Complete Statistical Sample of Edge-on Seyfert Galaxies

Galaxy Name	ROSAT Data?	Seyfert Type	D ^a (Mpc)
IC 1657		2	47.4
UM 319		2	63.1
Mrk 993		2	62.1
Mrk 577		2	69.1
Ark 79		2	68.8
NGC 931		1	66.6
NGC 1320		2	36.0
NGC 1386		2	20.0
NGC 2992	Yes	2	30.9
MCG –2-27-9		2	62.0
NGC 4235	Yes	1	32.1
NGC 4388	Yes	2	33.6
NGC 4602	Yes	1.9	34.0
NGC 4945	Yes	2	6.7
IC 4329A	Yes	1	63.9
NGC 5506	Yes	2	24.2
ESO 103-G35	Yes	2	53.1
NGC 6810		2	26.1
IC 1368		2	52.2
IC 1417		2	57.5
NGC 7410	Yes	2	23.3
NGC 7590	Yes	2	21.3

Optical positions, axial ratios and recessional velocities for these objects are listed in paper I, Table 1.

^aAssumed distance in Mpc. Except for NGC 1386 and NGC 4945, distances were calculated from recessional velocities listed in RC3 (see paper I), using $H_0 = 75$. The distance to NGC 1386 was taken as 20.0 Mpc (the distance to the Fornax cluster) and a distance of 6.7 Mpc was assumed for NGC 4945.

Table 2. **ROSAT Archival Data for Edge-on Seyfert Galaxies**

Galaxy Name	Offset ^a (arcmin)	Obs Date (YYMMDD)	Instr	Exp. ^b Time (s)	Cnts ^c	Count ^c Rate (10 ⁻² s ⁻¹)	10 ⁴⁰ erg s ⁻¹ Cnt Rate ^d (10 ⁻² s ⁻¹)	N _H ^{Gal,d} (10 ²⁰ cm ⁻²)
(1)	(2)	(3)	(4)	(5)	(6)	(7)	(8)	(9)
NGC 2992	0.3	931115–29	PSPC	18602	1781±44	9.6±0.2	0.7	5.5
	0.3	920523	HRI	10840	276±23	2.6±0.2	0.3	
NGC 4235	0.1	920701–07	PSPC	9142	1265±38	13.8±0.4	0.8	1.6
	0.1	921208–23	PSPC	10297	1819±45	17.7±0.4	0.8	
NGC 4388	0.5	930616–0707	PSPC	11650	344±23	3.0±0.2	0.7	3
	0.3	911207–09	HRI	11256	147±19	1.3±0.2	0.3	
NGC 4602	19.3	920714	PSPC	1261		<1.0	0.7	2.3
NGC 4945	0.1	920812–15	PSPC	14190	1426±66	10.1±0.5	11.6	14.5
	0.1	930710–11	PSPC	9028	1202±53	13.3±0.6	11.6	
IC 4329A	0.1	930114	PSPC	8230	22324±151	271±2	0.2	4.6
NGC 5506	0.3	920124–27	PSPC	4462	1209±36	27.1±0.8	1.2	4.2
	0.3	940710–28	HRI	18019	866±36	4.8±0.2	0.5	
ESO 103–G35	4.6	930331–0413	PSPC	16813	73±13	0.4±0.1	0.2	7.6
NGC 7410	0.2	931203	PSPC	1491		<1.1	1.6	1.3
NGC 7590	10.1	930504–05	PSPC	7241	107±14	1.5±0.2	1.8	2.0

^aDifference between optical position of galaxy (see paper I) and pointing center of observation

^bNet exposure time of observation

^cNet (background-subtracted) counts and count rates from the galaxy (see text for more details)

^d Sample count rates (for comparison) of a hypothetical source with a 0.2–2.4 keV luminosity of 10⁴⁰ erg s⁻¹, located at the distance of the galaxy. We have assumed a thermal spectrum and have taken into account absorption of soft X-rays due to the the Galactic column toward the galaxy. Galactic columns (column 9) were taken from Elvis, Lockman, & Wilkes (1989), Boller et al. 1992, Iwasawa et al. 1996, and Dickey & Lockman 1990.

Table 3. X-ray Images of Edge-on Seyfert Galaxies

Galaxy Name	Scale ^a (kpc arcmin ⁻¹)	Fig No. ^b	Comment ^b
NGC 2992	9.00	1a	HRI extended
NGC 4235	9.36	...	PSPC only, unresolved
NGC 4388	9.78	1b,c	PSPC extended
NGC 4945	1.95	1d	PSPC only, no extended emission ^c
IC 4329A	18.60	2a	PSPC only, unresolved
NGC 5506	7.02	2b,c	Extended
ESO 103-G35	15.42	...	PSPC only, weak nucleus, unresolved
NGC 7590	6.18	...	PSPC only, weak nucleus, unresolved

^aLinear scale using assumed distances listed in Table 1

^bFigure number for contour plots of ROSAT images and comment about whether extended emission is apparent in the image

^cThe Galactic column toward NGC 4945 is very high ($N_H \gtrsim 10^{21} \text{ cm}^{-2}$) and any extended soft X-ray emission with temperatures $\lesssim 1-2 \text{ keV}$ would be significantly absorbed.

Table 4. **Dimensions and Count Rates of Extended X-ray Emission**

Galaxy	Radius ^a		Orientation ^b		Instr	Cnts ^c	Cnt Rate ^c
	(arcsec)	(kpc)	P.A. (deg)	Half Angle (deg)			
NGC 2992	35–45	5.3–6.8	110	10	HRI	11±5	0.10±0.04
NGC 4388	<85	<13.6	65	65	PSPC	113±28	1.0±0.2
NGC 5506	10–25	1.2–3.0	–20	45	HRI	72±13	0.40±0.08

^aRange of radii of extended X-ray emission.

^bOrientation of large-scale X-ray structure with respect to the nuclear X-ray source. P.A. and opening angle (half angle).

^cNet counts and net count rate of extended emission

Table 5. **Properties of the Extended X-ray Emitting Gas**

Galaxy Name	V $\times 10^{65}$ (cm^3)	kT (keV)	L_X $\times 10^{41}$ (erg s^{-1})	$f n^2 V$ $\times 10^{62}$ (cm^{-3})	$f^{\frac{1}{2}} n$ $\times 10^{-2}$ (cm^{-3})	$f^{\frac{1}{2}} 2nkT$ $\times 10^{-11}$ (dyne cm^{-2})	$f^{-\frac{1}{2}} t_{cool}$ $\times 10^7$ (yr)
(1)	(2)	(3)	(4)	(5)	(6)	(7)	(8)
NGC 2992	1.5	1.0	0.04	0.93	2.4	7.9	10
		0.1	0.21	5.4	5.9	1.9	0.43
NGC 4388	890	1.0	0.15	3.8	0.21	0.66	120
		0.1	0.22	5.5	0.25	0.08	10
NGC 5506	4.6	1.0	0.09	2.1	2.2	7.0	12
		0.1	0.35	8.7	4.4	1.4	0.58

Derived Properties of the X-ray gas for two different cases: $kT = 1.0$ keV and $kT = 0.1$ keV (column 3). Columns are as follows: (1) name of galaxy, (2) volume of X-ray emitting gas in units of 10^{65} cm^3 , assuming the emitting region has a conical geometry (see text section 4.2), (3) assumed temperature in keV, (4) 0.2–2.4 keV X-ray luminosity in units of $10^{41} \text{ erg s}^{-1}$, (5) volume integral of the density squared in units of 10^{62} cm^3 , calculated from the X-ray luminosity and the ROSAT emissivity from Suchkov et al. 1994, (6) density $f^{\frac{1}{2}} n$ in units of 10^{-2} cm^{-3} , where f is the filling factor of the X-ray gas in the volume, (7) pressure $f^{\frac{1}{2}} 2nkT$ in units of $10^{-11} \text{ dyne cm}^{-2}$, and (8) cooling time of the X-ray gas $f n V k T / L_X$ in units of 10^7 yr. See text section 4.2 for additional details.

REFERENCES

- Antonucci, R. R. J. 1993, *ARA&A*, 31, 473
- Baum, S. A., O’Dea, C. P., Dallacassa, D., de Bruyn, A. G., & Pedlar, A. 1993, *ApJ*, 419, 553
- Biretta, J. 1993, in *Astrophysical Jets*, ed. D. Burgarella, M. Livio & C. P. O’Dea (Cambridge: Cambridge University Press), p. 263
- Boller, Th., Meurs, E. J. A., Brinkmann, W., Fink, H., Zimmerman, U., & Adorf, H.-M. 1992, *A&A*, 261, 57
- Bregman, J. N., & Houck, J. C. 1997, *ApJ*, 485, 159
- Colbert, E. J. M., Baum, S. A., Gallimore, J. F., O’Dea, C. P., & Christensen, J. A. 1996a, *ApJ*, 467, 551 (Paper II)
- Colbert, E. J. M., Baum, S. A., Gallimore, J. F., O’Dea, C. P., Lehnert, M. D., Tsvetanov, Z. I., Mulchaey, J. S., & Caganoff, S. 1996b, *ApJS*, 105, 75 (Paper I)
- Dickey, J. M., & Lockman, F. J. 1990, *ARA&A*, 28, 215
- Elvis, M., Lockman, F. J., & Wilkes, B. J. 1989, *AJ*, 97, 777
- Heckman, T. M., Armus, L., & Miley, G. K. 1990, *ApJS*, 74, 833
- Heckman, T. M., Gonzalez-Delgado, R., Leitherer, C., Meurer, G. R., Krolik, J., Wilson, A. S., Koratkar, A., & Kinney, A. 1997, *ApJ*, 482, 114
- Heckman, T. M., Krolik, J., Meurer, G. R., Calzetti, D., Kinney, A., Koratkar, A., Leitherer, C., Robert, C., & Wilson, A. S. 1995, *ApJ*, 452, 549
- Krolik, J. H., & Begelman, M. C. 1986, *ApJ*, 308, L55
- Krolik, J. H., & Vrtilik, J. M. 1984, *ApJ*, 279, 521
- Matt, G., Piro, L., Antonelli, L. A., Fink, H. H., Meurs, E. J. A., & Perola, G. C. 1994, *A&A*, 292, 13
- Morse, J. M. 1994, *PASP*, 106, 675
- Nousek, J. A., & Lesser, A. 1993, in *ROSAT Newsletter No. 8*, p.13
- Raymond, J. C., & Smith, B. 1977, *ApJS*, 35, 419
- Robinson, A. 1994, *A&A*, 291, 351
- Robinson, A. 1989, in “Extranuclear Activity in Galaxies,” eds. E. Meurs & R. Fosbury (Garching:ESO), p. 250
- Ryder, S. D., Staveley-Smith, L., Dopita, M., Petre, R., Colbert, E., Malin, D., & Schlegel, E. 1993, *ApJ*, 416, 167

- Seaquist, E. R., & Odegard, N. 1991, *ApJ*, 369, 320
- Suchkov, A. A., Balsara, D. S., Heckman, T. M., & Leitherer, C. 1994, *ApJ*, 430, 511
- Turner, T. J., Weaver, K. A., Mushotzky, R. F., Holt, S. S., & Madejski, G. M. 1991, *ApJ*, 381, 85
- van der Laan, H. & Perola, G. C. 1969, *A&A*, 3, 468
- Weaver, K. A., Mushotzky, R. F., Serlemitsos, P. J., Wilson, A. S., Elvis, M., & Briel, U. 1995, *ApJ*, 442, 597
- Weaver, K. A., Nousek, J., Yaqoob, T., Mushotzky, R. F., Makino, F., & Otani, C. 1996, *ApJ*, 458, 160
- Wilson, A. S. 1994, in *The Soft X-ray Cosmos: Proc. of the ROSAT Science Symposium*, ed. E. Schlegel & R. Petre (AIP: New York), p. 115

Fig. 1.— **NGC 2992.** (a, top left) ROSAT HRI contours over grayscale plot of B-band GASP image (from the STScI digitized sky-survey). The HRI image was smoothed with a Gaussian kernel of $\sigma = 24''$. **NGC 4388.** (b, top right) ROSAT HRI contours over grayscale plot of B-band GASP image. The HRI image was smoothed with a Gaussian kernel of $\sigma = 8''$. (c, bottom left) ROSAT PSPC contours over grayscale plot of B-band GASP image. **NGC 4945.** (d, bottom right) ROSAT PSPC contours over grayscale plot of B-band GASP image.

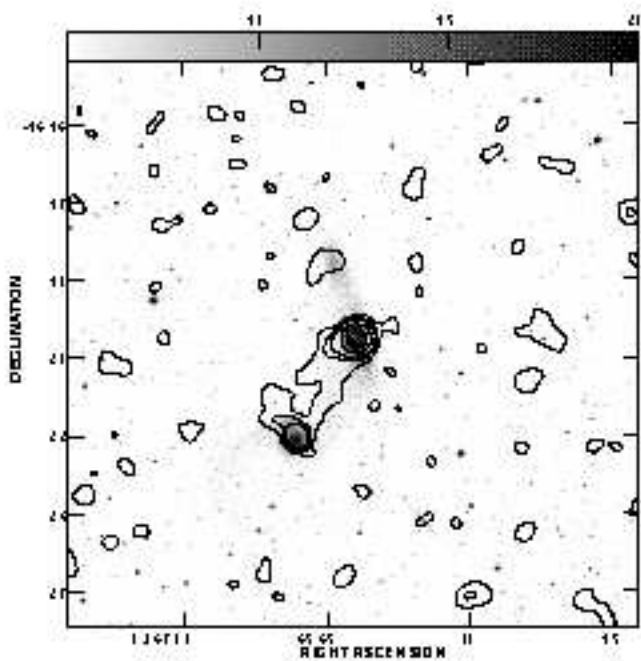
Fig. 2.— **IC 4329A.** (a, top left) ROSAT PSPC contours over grayscale plot of B-band GASP image. **NGC 5506.** (b, top right) ROSAT PSPC contours over grayscale plot of B-band GASP image. (c, bottom left) ROSAT HRI contours over grayscale plot of B-band GASP image. The HRI image was smoothed with a Gaussian kernel of $\sigma = 24''$.

Fig. 3.— **Radial Profiles of X-ray Emission from NGC 2992.** Radial profiles in units of counts per $4''$ pixel for four quadrants. Symbols are as follows: open triangles, PA = $-30^\circ - 60^\circ$; open rectangles, PA = $60^\circ - 150^\circ$; open pentagons, PA = $150^\circ - 240^\circ$; open hexagons, PA = $240^\circ - 330^\circ$. Error bars are 1σ of the total number of counts. (a) 20 counts per radial bin. Note the clear excess emission in the 2nd quadrant ($60^\circ - 150^\circ$). (b) 10 counts per radial bin. Again, the excess emission manifests itself at the same radii ($\sim 35'' - 45''$).

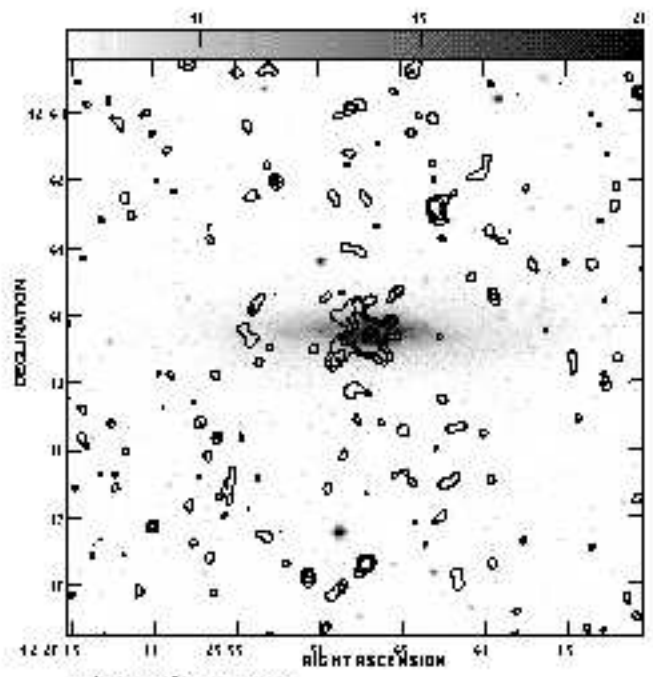
Fig. 4.— **Radial Profile of Extended X-ray Emission from NGC 5506.** A model PSF (solid line) from an observation of HZ43 is also shown for comparison.

Fig. 5.— **Extended radio and X-ray emission in NGC 2992.** Contours are 1.4 GHz (20 cm) radio continuum emission (see paper II) and grayscale is the ROSAT HRI soft X-ray image (see Figure 1a), displayed on a logarithmic scale to bring out the faint features. The lowest surface brightness levels displayed from the X-ray image are $\sim 1 \times 10^{-2}$ cts s^{-1} arcmin $^{-2}$. The arrows show the orientation of the galaxy disk. Axis coordinates are epoch B1950.

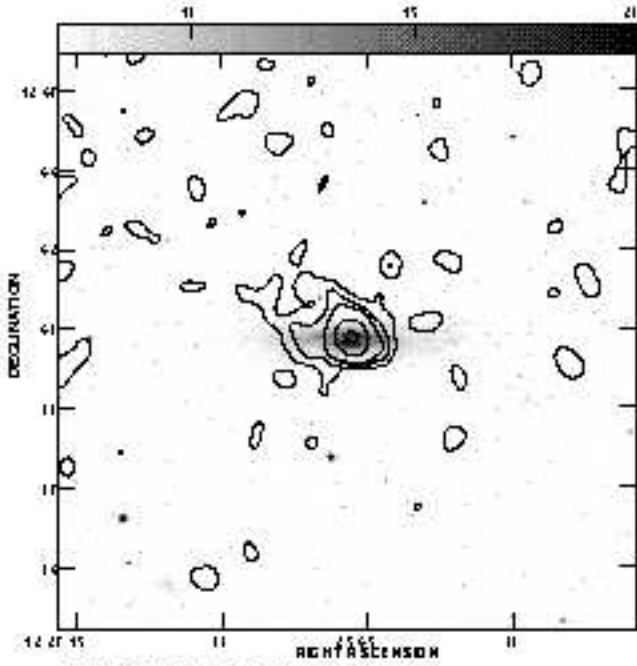
Fig. 6.— **Extended radio and X-ray emission in NGC 5506.** Contours are soft X-ray emission from the ROSAT HRI image (improved using the techniques of Morse 1994) and grayscale is from a 4.9 GHz radio continuum image (paper II). The greyscale image is displayed on a logarithmic scale to bring out the structure of the extended radio emission. The lowest surface brightness levels displayed from the radio image are $\sim 50 \mu\text{Jy beam}^{-1}$ (beam size 5" FWHM). The arrows show the orientation of the galaxy disk (horizontal arrows in the ps figure are missing).



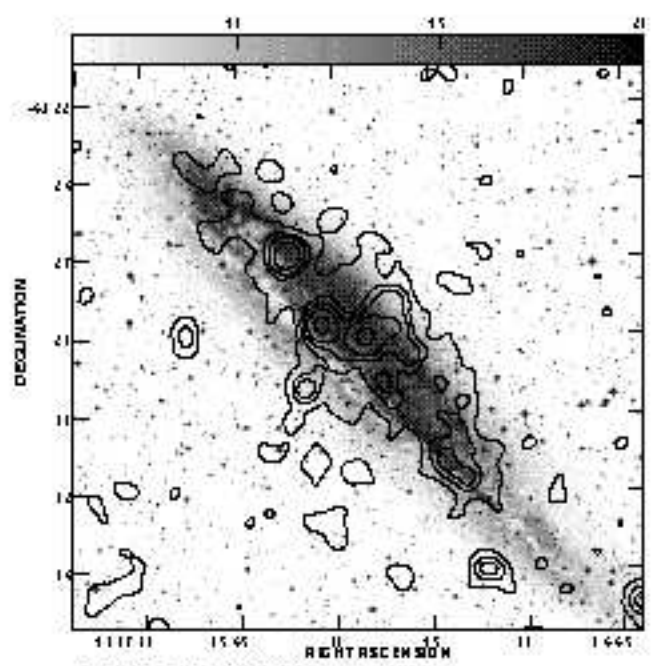
Peak of Source No. 1.1112E-11
 Size: 2.000E-11 * 1.00 1.00 1.00
 YIP: 2.00



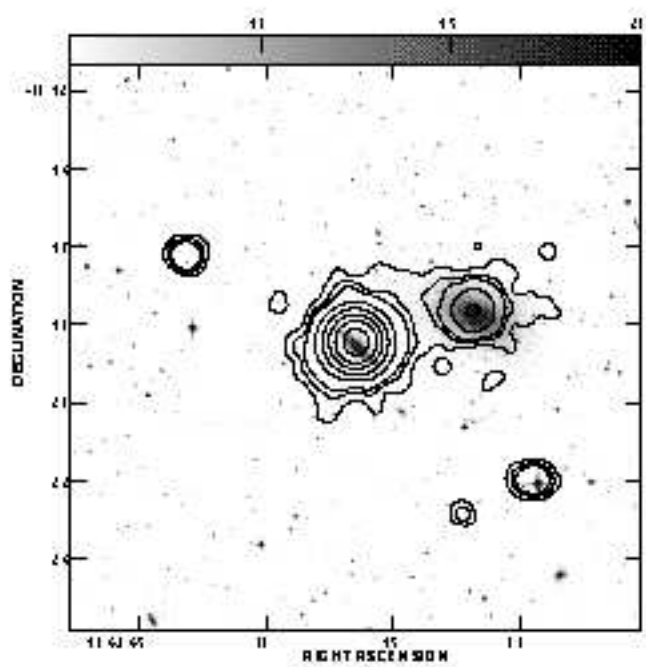
Peak of Source No. 1.9219E-11
 Size: 2.000E-11 * 1.00 1.00 1.00
 YIP: 2.00



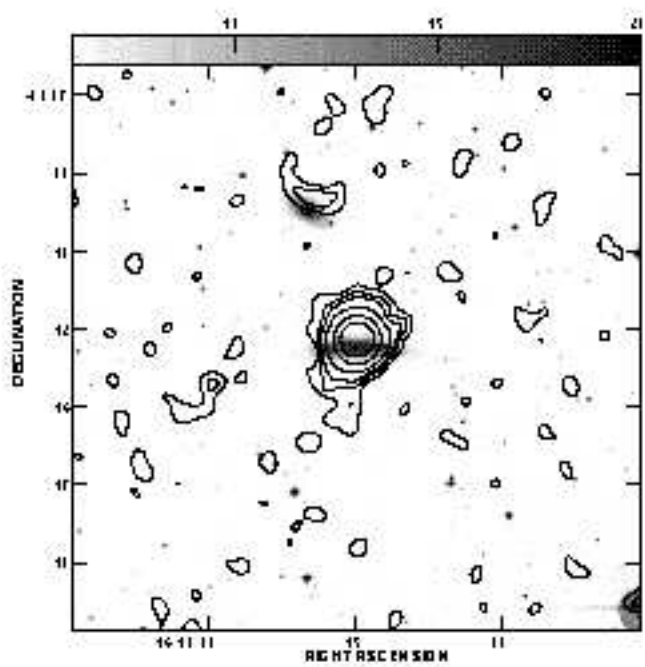
Peak of Source No. 2.0721E-11
 Size: 2.000E-11 * 1.20 1.00 1.00
 YIP: 2.00



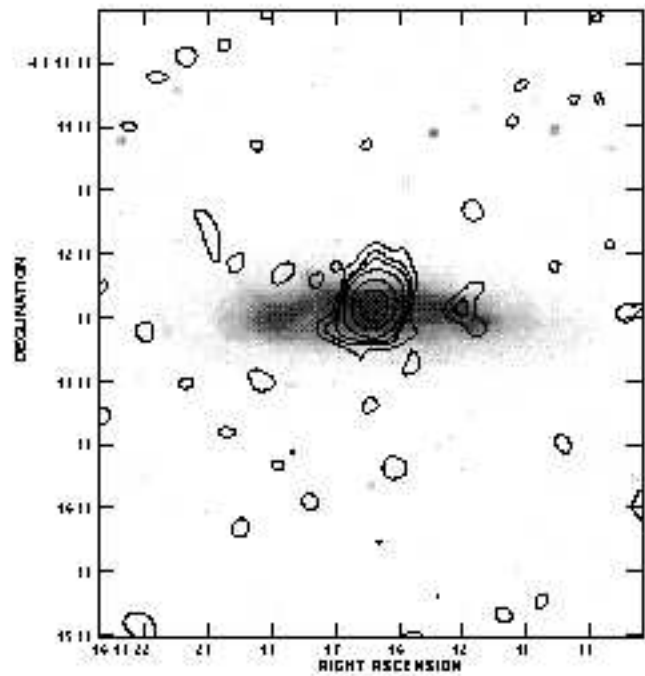
Peak of Source No. 1.2512E-11
 Size: 2.000E-11 * 1.00 1.00 1.00
 YIP: 2.00



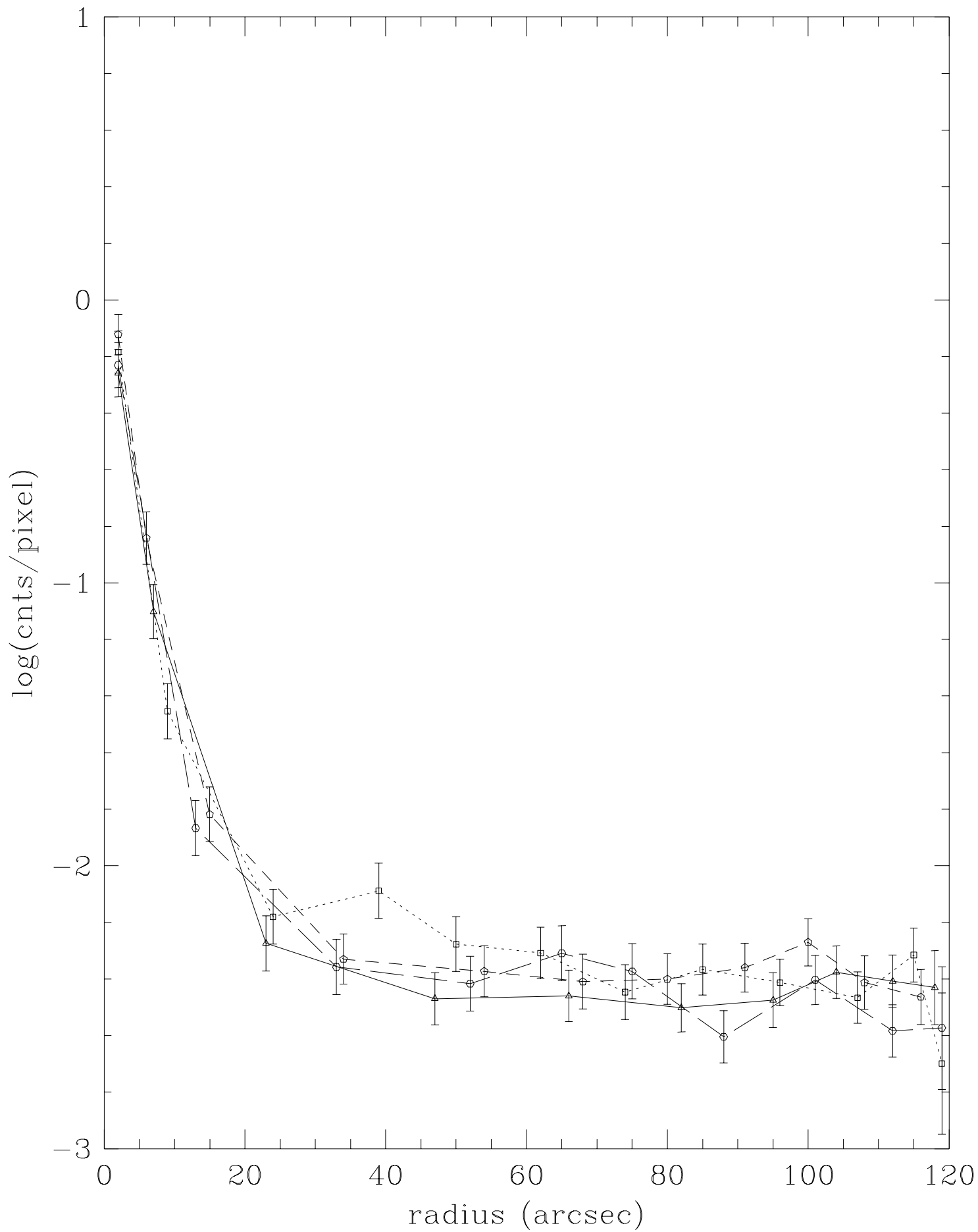
Peak 1: RA 11 42 10, Dec 10 15
 Peak 2: RA 11 42 12, Dec 10 14

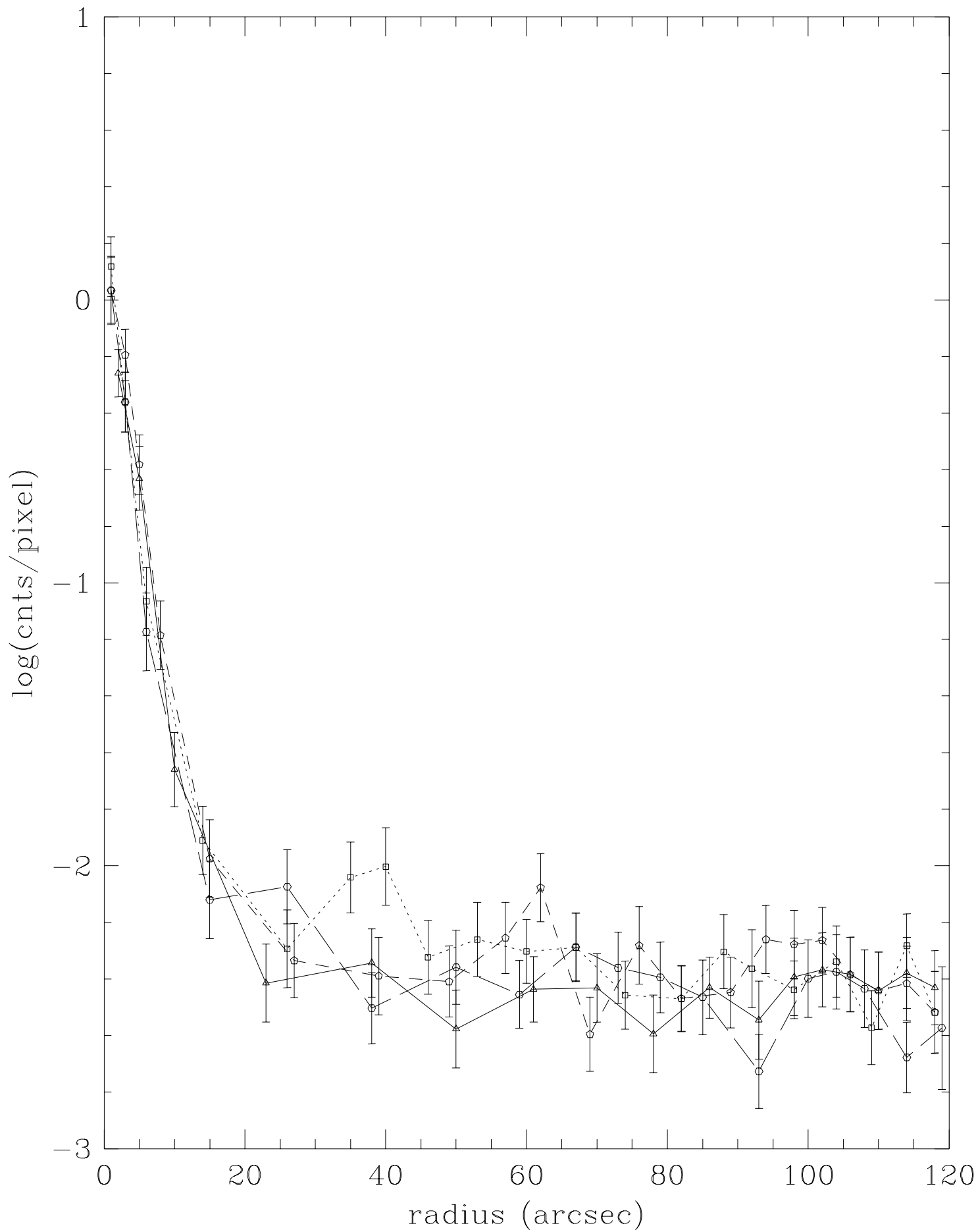


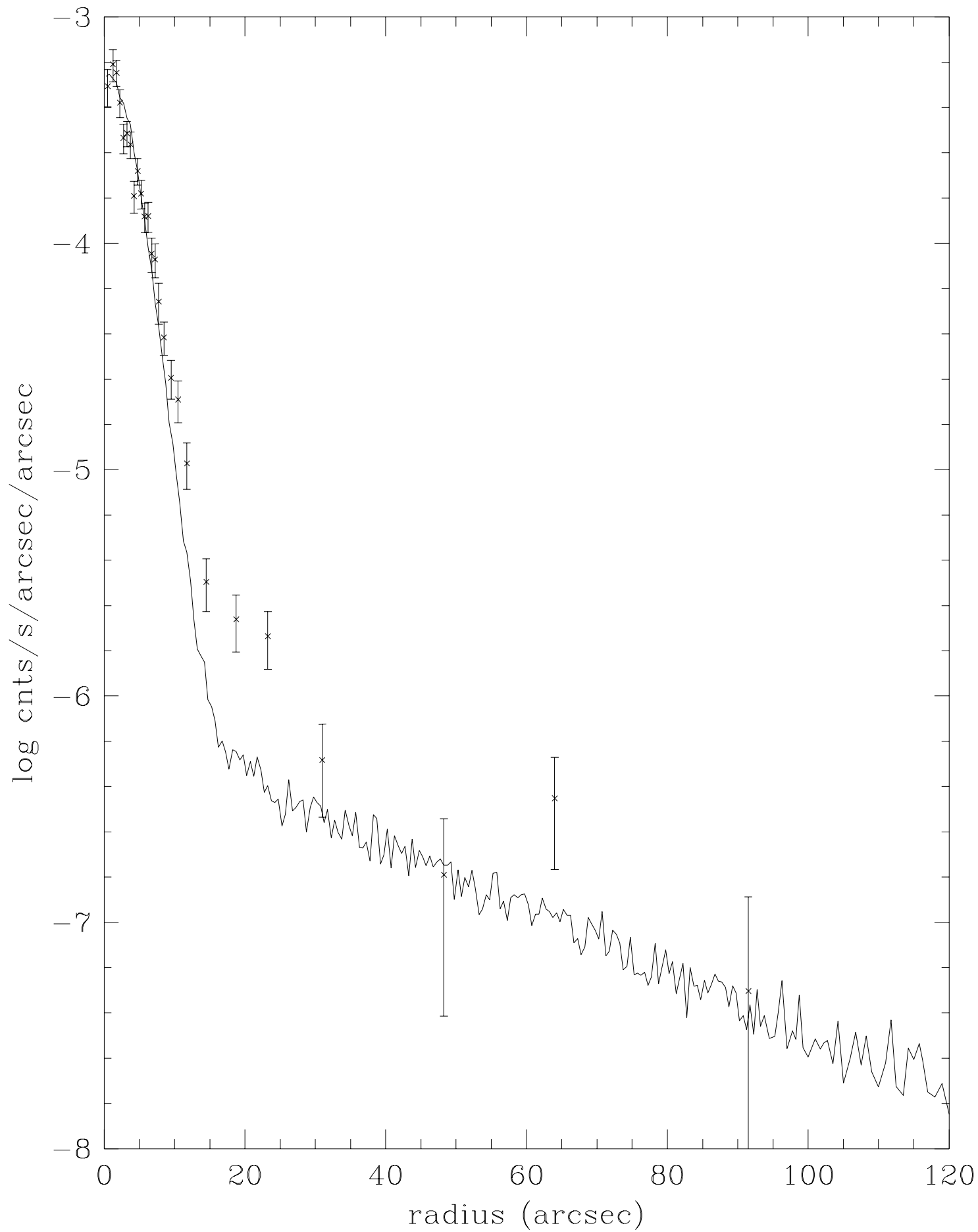
Peak 1: RA 16 41 15, Dec 11 15
 Peak 2: RA 16 41 15, Dec 11 15

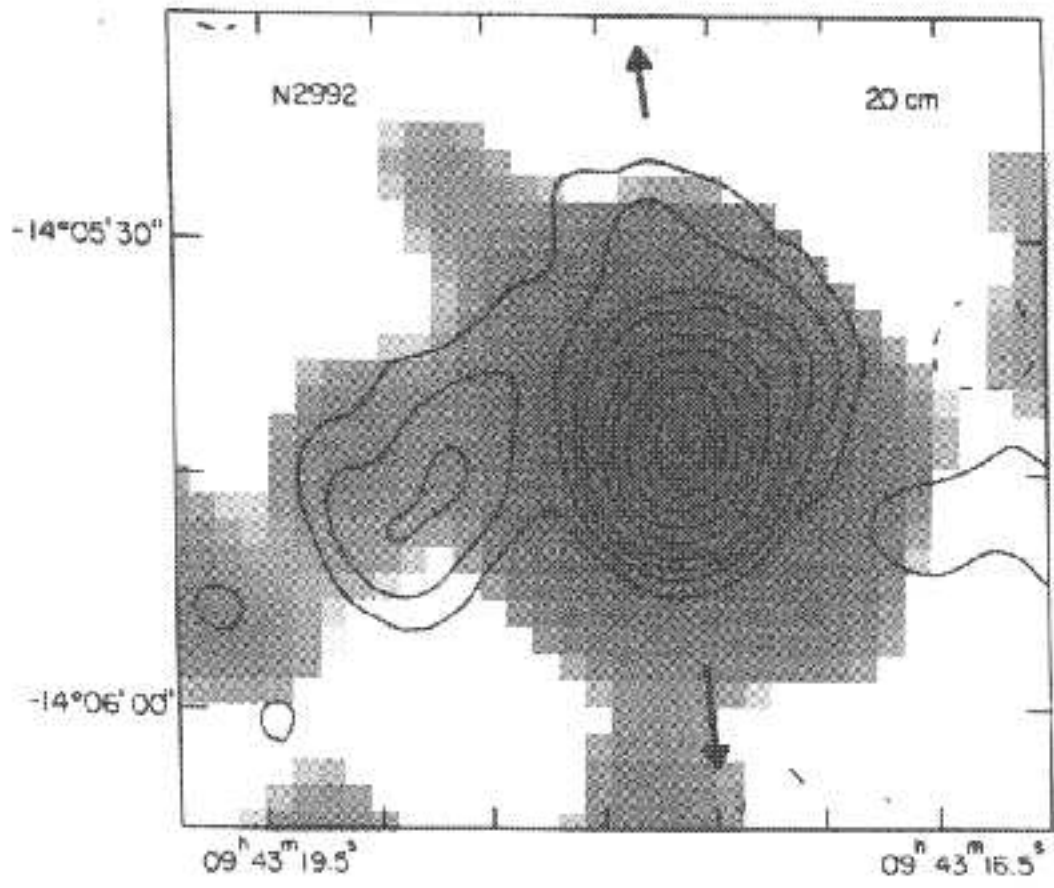


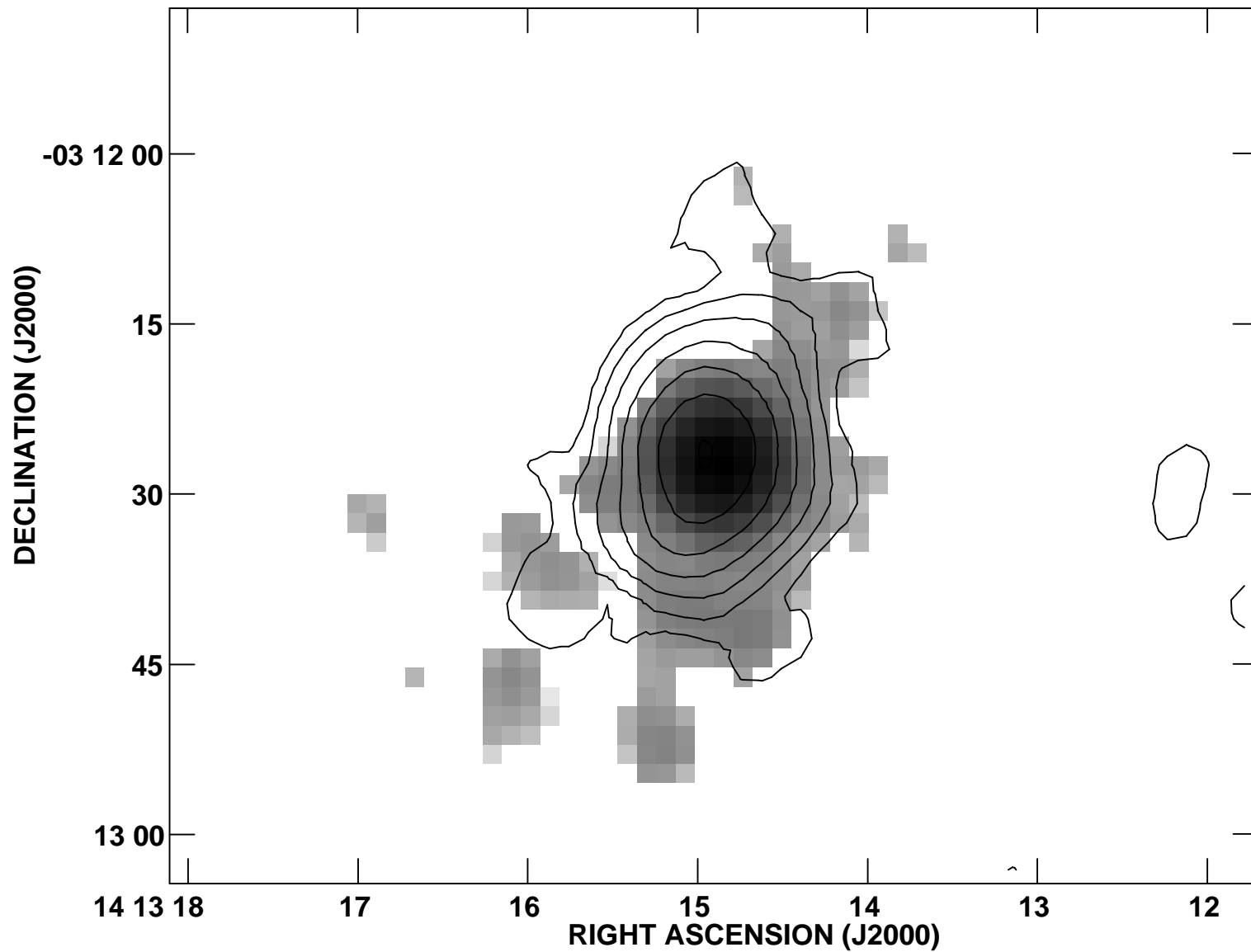
Peak 1: RA 16 41 15, Dec 11 15
 Peak 2: RA 16 41 15, Dec 11 15











Peak contour flux = 2.6680E+01
Levs = 1.0000E+00 * (0.400, 0.800, 1.600,
3.200, 6.400, 12.80, 25.60)